FMM-Modeling of Acoustic Scattering with Geometrical Uncertainty

Péter Fiala[1], Péter Rucz[1]

[1] *Laboratory of Acoustics, Budapest University of Technology and Economics, 1117 Budapest, Hungary, Email: fiala@hit.bme.hu*

Introduction

The scattering of sound fields from surfaces with geometrical uncertainties plays an important role in engineering acoustics. Possible applications include ultrasonic reflection from rough grounds, but the field is also important in acoustic localization or shape optimization. In the present context, the topic is investigated from the aspect of uncertainty quantification and uncertainty propagation. Given the amount of uncertainty in the description of the scatterer's surface, we search for the characterization of the uncertainty in the scattered field. The main modeling challenge in the field of scattering from random surfaces is the inherent nonlinearity in the system: the dependence of the scattered field on the scatterer's geometry is highly nonlinear.

Analytical solutions only exist for the limiting cases of infinitesimally small deformations. For real life-like applications, Monte Carlo Simulation methods may be applied to assess the uncertainty in the scattered field. However, their application requires the solution of a huge number of independent systems, in order to reach convergence. Alternatively, Polynomial Chaos Expansion techniques, like Stochastic Galerkin [1] and Stochastic Collocation [2] methods can be applied to compute the statistics of the scattered field. These methods are based on the Polynomial decomposition of the surface roughness, and express the scattered field in a similar polynomial decomposition. The choice of orthogonal polynomials can accelerate the solution procedure, but one soon faces the so-called 'curse of dimensionality' for processes with rapid random fluctuations.

In the present paper, we apply the perturbation method [3] to relate the covariance of the scattered field to that of the surface scatterer. The advantage of the perturbation method is that—opposed to the application of the previously mentioned techniques—the solution is boiled down to independent solution of similar exterior problems defined on the same geometry. In other words, the perturbation method reduces the exterior problem with uncertain geometry to an exterior problem with lots of uncertain excitations.

The Fast Multipole Method (FMM) is applied in a twofold way. On one hand, it is used to accelerate the decomposition of the random roughness into a first order PCE, on the other hand, the FMM is used to solve exterior acoustic problems.

Methodology

Scattering of an incident field from a sound-soft scatterer with uncertain geometry is described by the Boundary Value Problem (BVP)

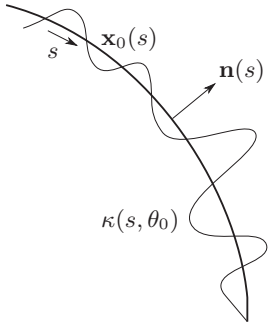

Figure 1: The uncertain scatterer geometry

$$\left(\nabla^2 + k^2\right) p(\mathbf{x},\theta) = 0, \quad \mathbf{x} \in \Omega_e \tag{1}$$

$$p(\mathbf{x},\theta) = -p_{\text{inc}}(\mathbf{x}), \quad \mathbf{x} \in \Gamma(\theta) \tag{2}$$

where p_{inc} denotes the incident field, and p denotes the scattered field. The scattered field satisfies the Helmholtz equation (1) in the external domain Ω_e, and satisfies the Dirichlet Boundary Condition (BC) (2) on the boundary Γ. $k = \omega/c$ denotes the acoustic wave number, where ω is the angular frequency and c denotes speed of sound.

The uncertain boundary $\Gamma(\theta)$—where θ denotes dependency on a random event—is characterized by a mean boundary Γ_0 and small magnitude normal perturbation $\kappa(\mathbf{x},\theta)$ superposed on the mean boundary Γ_0, as shown in Figure 1 [4]. The magnitude of the deformation is controlled by the parameter $0 < \epsilon \ll 1$:

$$\Gamma_\epsilon(\theta) = \{\mathbf{x} + \epsilon \mathbf{n}(\mathbf{x})\kappa(\mathbf{x},\theta)\} \tag{3}$$

where $\mathbf{n}(\mathbf{x})$ is the outward unit normal of the mean boundary.

Input and Output Statistics

It is assumed that the deformation process is of zero mean $\mathrm{E}_\kappa(\mathbf{x}) = \mathrm{E}\kappa(\mathbf{x},\theta) = 0$, otherwise the mean boundary Γ_0 could be modified accordingly. The deformation is further characterized by its two-point correlation function $\mathrm{Corr}_\kappa(\mathbf{x},\mathbf{y})$, which, for the zero mean case is equal to the covariance:

$$\mathrm{Corr}_\kappa(\mathbf{x},\mathbf{y}) = \mathrm{Cov}_\kappa(\mathbf{x},\mathbf{y}) = \mathrm{E}\kappa(\mathbf{x},\theta)\kappa(\mathbf{y},\theta) \tag{4}$$

The uncertain deformation of the scatterer introduces uncertainty into the scattered pressure field p. In the followings, the first and second order statistics of the scattered field will be determined, namely its expectation $\mathrm{E}_p(\mathbf{x}) = \mathrm{E}p(\mathbf{x},\theta)$ and two-point correlation $\mathrm{Corr}_p(\mathbf{x},\mathbf{y}) = \mathrm{E}p(\mathbf{x},\theta)\bar{p}(\mathbf{y},\theta)$, where the bar above a complex number denotes its complex conjugate.

Perturbation Method for the Scattered Field

Assuming small perturbations of the boundary ($\epsilon \ll 1$), any smooth function $\varphi(\mathbf{x})$ on the perturbed boundary Γ_ϵ can be expanded into a Taylor series around the mean boundary Γ_0 as follows:

$$\begin{aligned}\varphi(\mathbf{x}+\epsilon\mathbf{n}(\mathbf{x})\kappa(\mathbf{x},\theta)) &= \sum_{k=0}^{\infty}\frac{1}{k!}\frac{\partial^k\varphi(\mathbf{x})}{\partial n^k}\epsilon^k\kappa(\mathbf{x})^k \\ &= \varphi(\mathbf{x})+\epsilon\partial_n\varphi(\mathbf{x})\kappa(\mathbf{x},\theta)+\epsilon^2\frac{1}{2}\partial_n^2\varphi(\mathbf{x})\kappa^2(\mathbf{x},\theta)+O(\epsilon^3)\end{aligned} \tag{5}$$

where ∂_n denotes derivative with respect to the normal.

The uncertain scattered field $p(\mathbf{x},\theta)$ is expanded into a power series of the roughness magnitude ϵ as follows:

$$\begin{aligned}p_\epsilon(\mathbf{x},\theta) &= \sum_{n=0}^{\infty}\epsilon^n p_n(\mathbf{x},\theta) \\ &= p_0(\mathbf{x})+\epsilon p_1(\mathbf{x},\theta)+\epsilon^2 p_2(\mathbf{x},\theta)+O(\epsilon^3)\end{aligned} \tag{6}$$

where p_0 denotes the scattered field for the nominal problem (mean geometry), and subsequent terms contribute to its stochastic perturbations.

The power series (6) results in the following second order expressions for the expectation and two-point correlation of the pressure field:

$$\mathrm{E}_p(\mathbf{x}) = p_0(\mathbf{x})+\epsilon\mathrm{E}p_1(\mathbf{x},\theta)+\epsilon^2\mathrm{E}p_2(\mathbf{x},\theta)+O(\epsilon^3) \tag{7}$$

$$\begin{aligned}\mathrm{Corr}_p(\mathbf{x},\mathbf{y}) &= p_0(\mathbf{x})\bar{p}_0(\mathbf{y})+\epsilon\left(p_0(\mathbf{x})\mathrm{E}_{\bar{p}_1}(\mathbf{y})+\mathrm{E}_{p_1}(\mathbf{x})\bar{p}_0(\mathbf{y})\right) \\ &+\epsilon^2\left(\mathrm{Corr}_{p_1}(\mathbf{x},\mathbf{y})+p_0(\mathbf{x})\mathrm{E}_{\bar{p}_2}(\mathbf{y})+\mathrm{E}_{p_2}(\mathbf{x})\bar{p}_0(\mathbf{y})\right)+O(\epsilon^3)\end{aligned} \tag{8}$$

Finally, the two-point covariance takes the simple form

$$\mathrm{Cov}_p(\mathbf{x},\mathbf{y}) = \epsilon^2\mathrm{Cov}_{p_1}(\mathbf{x},\mathbf{y})+O(\epsilon^3) \tag{9}$$

Substituting the second order power series expansion (6) into the BVP (1)-(2) and applying (5) for the approximation of the pressure field p and the incident field p_{inc} on the boundary Γ_ϵ results in a series of boundary value problems on the mean geometry Γ_0.

The zero-th order deterministic BVP (10)-(11) describes the nominal pressure field $p_0(\mathbf{x})$

$$\left(\nabla^2+k^2\right)p_0(\mathbf{x}) = 0, \quad \mathbf{x}\in\Omega_e \tag{10}$$

$$p_0(\mathbf{x}) = -p_{\mathrm{inc}}(\mathbf{x}), \quad \mathbf{x}\in\Gamma_0 \tag{11}$$

The first order perturbed field $p_1(\mathbf{x},\theta)$ is the solution of the stochastic BVP

$$\left(\nabla^2+k^2\right)p_1(\mathbf{x},\theta) = 0, \quad \mathbf{x}\in\Omega_e \tag{12}$$

$$p_1(\mathbf{x},\theta) = -\partial_n\left(p_{\mathrm{inc}}(\mathbf{x})+p_0(\mathbf{x})\right)\kappa(\mathbf{x},\theta), \quad \mathbf{x}\in\Gamma_0 \tag{13}$$

Apparently, the boundary condition of the first order BVP depends on the solution p_0 of the mean system. As the excitation of the first order linear system is of zero mean, so is the solution: $\mathrm{E}_{p_1}(\mathbf{x}) = 0$. This simplifies the statistics of the solution (7), (8).

The second order perturbation field $p_2(\mathbf{x},\theta)$ satisfies the BVP

$$\left(\nabla^2+k^2\right)p_2(\mathbf{x},\theta) = 0, \quad \mathbf{x}\in\Omega_e \tag{14}$$

$$\begin{aligned}p_2(\mathbf{x},\theta) = -\Big(&\frac{1}{2}\partial_n^2\left(p_{\mathrm{inc}}(\mathbf{x})+p_0(\mathbf{x})\right)\kappa^2(\mathbf{x},\theta) \\ &+\partial_n p_1(\mathbf{x},\theta)\kappa(\mathbf{x},\theta)\Big), \quad \mathbf{x}\in\Gamma_0\end{aligned} \tag{15}$$

Taking the expectation of (14)-(15) results in a deterministic BVP for $\mathrm{E}_{p_2}(\mathbf{x})$:

$$\left(\nabla^2+k^2\right)\mathrm{E}_{p_2}(\mathbf{x}) = 0, \quad \mathbf{x}\in\Omega_e \tag{16}$$

$$\begin{aligned}\mathrm{E}_{p_2}(\mathbf{x}) = -&\frac{1}{2}\partial_n^2\left(p_{\mathrm{inc}}(\mathbf{x})+p_0(\mathbf{x})\right)\mathrm{D}_\kappa^2(\mathbf{x}) \\ &-\mathrm{Cov}_{\partial_n p_1\kappa}(\mathbf{x}), \quad \mathbf{x}\in\Gamma_0\end{aligned} \tag{17}$$

where $\mathrm{D}_\kappa^2(\mathbf{x}) = \mathrm{Cov}_\kappa(\mathbf{x},\mathbf{x})$ is the variance of the deformation field.

Decomposition of the Deformation Input

For further simplification of the above description, the stochastic deformation κ of the boundary is decomposed into its truncated Karhunen-Loève (KL) expansion:

$$\kappa(\mathbf{x},\theta) = \sum_{n=1}^{L}\sqrt{\lambda_n}g_n(\mathbf{x})\xi_n(\theta) \tag{18}$$

where ξ_n denote uncorrelated random variables, and $g_n(\mathbf{x})$ denote the eigenfunctions of the covariance function $\mathrm{Cov}_\kappa(\mathbf{x},\mathbf{y})$ with the corresponding eigenvalues λ_n:

$$\int_{\Gamma_0}\mathrm{Cov}_\kappa(\mathbf{x},\mathbf{y})g_n(\mathbf{y})\mathrm{d}\mathbf{y} = \lambda_n g_n(\mathbf{x}) \tag{19}$$

The introduction of a truncated KL-decomposition with the truncation limit L reduces the stochastic BVP (12)-(13) into L independent deterministic BVP as follows:

$$p_1(\mathbf{x},\theta) = \sum_{n=1}^{L}\sqrt{\lambda_n}p_1^n(\mathbf{x})\xi_n(\theta), \tag{20}$$

where

$$\left(\nabla^2+k^2\right)p_1^n(\mathbf{x}) = 0, \quad \mathbf{x}\in\Omega_e \tag{21}$$

$$p_1^n(\mathbf{x}) = -\partial_n\left(p_{\mathrm{inc}}(\mathbf{x})+p_0(\mathbf{x})\right)g_n(\mathbf{x}), \quad \mathbf{x}\in\Gamma_0 \tag{22}$$

Furthermore, the excitation of the second order problem (17) is expressed as

$$\mathrm{Cov}_{\partial_n p_1\kappa}(\mathbf{x}) = \sum_{n=1}^{L}\lambda_n\partial_n p_1^n(\mathbf{x})g_n(\mathbf{x}) \tag{23}$$

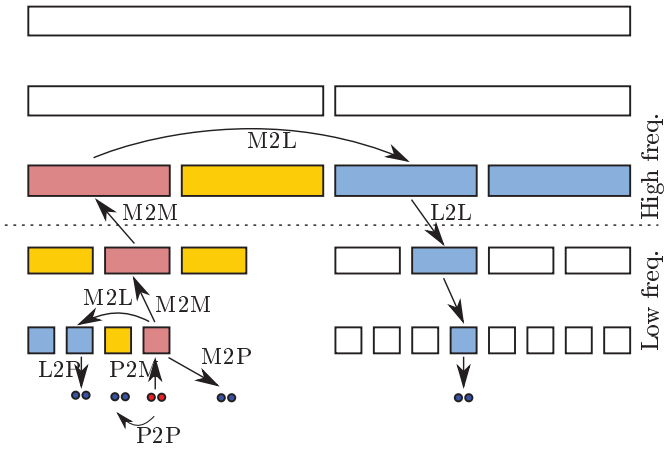

Figure 2: Schematic representation of information transfer in the FMM cluster tree

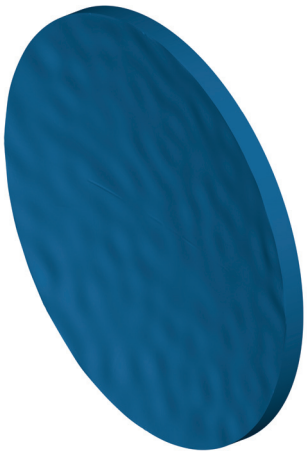

Figure 3: A parabolic focuser with a realization of the deformation field

Applications of the FMM

FMM for the Stochastic Eigendecomposition

The stochastic eigendecomposition problem (19) is solved numerically by a Galerkin discretization using local polynomial shape functions $N_i(\mathbf{x})$:

$$\sum_j \int_{\Gamma_0}\int_{\Gamma_0} N_i(\mathbf{x})\mathrm{Cov}_\kappa(\mathbf{x},\mathbf{y})N_j(\mathbf{y})\mathrm{d}\mathbf{y}\mathrm{d}\mathbf{x}\, g_{n,j} = \sum_j \lambda_n \int_{\Gamma_0} N_i(\mathbf{x})N_j(\mathbf{x})\mathrm{d}\mathbf{x}\, g_{n,j} \quad (24)$$

leading to a generalized discrete eigenvalue problem $\mathbf{D}\mathbf{g}_n = \lambda_n \mathbf{B}\mathbf{g}_n$. The matrix $\mathbf{B}$ on the right hand side is sparse. However, the matrix $\mathbf{D}$ is dense, and even the computation of all its entries is computationally inefficient. As an alternative, the Black Box Fast Multipole Method (bbFMM) [5] is applied to approximate matrix vector products $\mathbf{D}\mathbf{g}$ in an iterative eigensolver algorithm. The FMM decomposes the matrix vector product into near field and far field contributions, where the near field is computed directly by evaluating matrix entries, and the far field is approximated using a low rank approximation of the involved kernel. For the case of the Black Box FMM, asymptotically smooth kernels are assumed, and the low rank approximation is based on Chebyshev interpolation of the kernel function between far clusters. The information transfer of the multilevel FMM is schematically represented in Figure 2.

FMM for the Helmholtz Equation

After the stochastic eigendecomposition has been computed, the exterior Helmholtz problems on the reference boundary are solved using the Boundary Element Method for the Helmholtz equation. Discretization of the geometry into constant boundary elements reduces the exterior Dirichlet problem to the algebraic equations

$$\left(\mathbf{H}_s - \frac{1}{2}\mathbf{I}\right)\mathbf{p}_{\mathrm{inc}} = \mathbf{G}_s\partial_n\mathbf{p}_s \quad (25)$$

$$-\mathbf{H}_f\mathbf{p}_{\mathrm{inc}} - \mathbf{G}_f\partial_n\mathbf{p}_s = \mathbf{p}_f \quad (26)$$

where $\mathbf{p}_s$ and $\mathbf{p}_f$ denote the scattered field on the surface and in the exterior points, respectively. The application of the BEM for the above problems has the advantage, that the normal derivative of the pressure field—which is needed as an excitation of the next BEM problem—is an intermediate result of the solution procedure. The solution of the surface system (25) is performed with an iterative GMRES solver, where one matrix-vector product is approximated by the Wideband Fast Multipole Method for the Helmholtz equation [6], which uses the multipole expansion of the Helmholtz kernel in the low frequency range (small clusters) of the cluster tree, and its diagonal form in the high frequency range.

The generic algorithm of the FMM has been implemented in C++, exploiting template metaprogramming. The implementation is capable of hosting different FMM-methods (Black Box FMM, Kernel-dependent FMM) with the same template framework. The code is parallelized using openMP. For the near field BEM computations, the generic C++ BEM template library NiHu [7] has been applied.

Numerical Examples

In order to demonstrate the capabilities of the method, the scattering from a parabolic scatterer of diameter $D = 2$ m was modelled. The scatterer mesh, consisting of 123,000 constant tria elements, is shown in Figure 3. The scatterer is assumed to be sound soft, and is illuminated from the normal direction by an acoustic plane wave with wave number $kD = 40$. This acoustic wave number does not necessitate the application of a very fine mesh. The fine mesh ensures that random geometrical deformations with small characteristic lengths can be mdoelled with good accuracy.

The deformation field on the scatterer surface is characterized by an exponential correlation

$$\mathrm{Corr}_\kappa(r) = \sigma^2 \mathrm{e}^{-r/d_{\mathrm{corr}}} \quad (27)$$

where r is the distance between two points on the scatterer, and d_{corr} is the correlation length. The standard

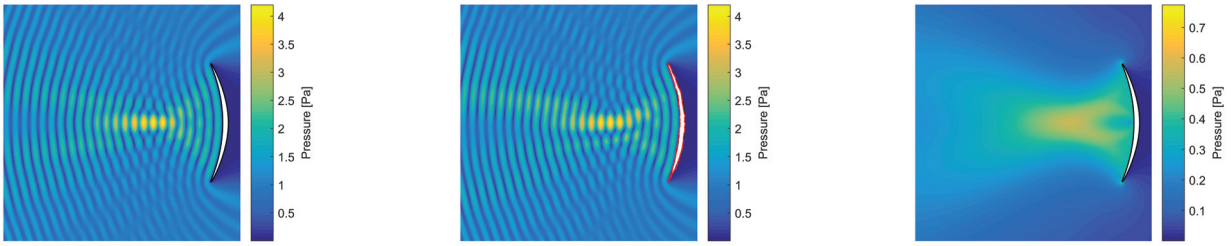

(a) (b) (c)

Figure 4: The scattered field. (a) the mean scattered field (b) its one realization (c) the standard deviation

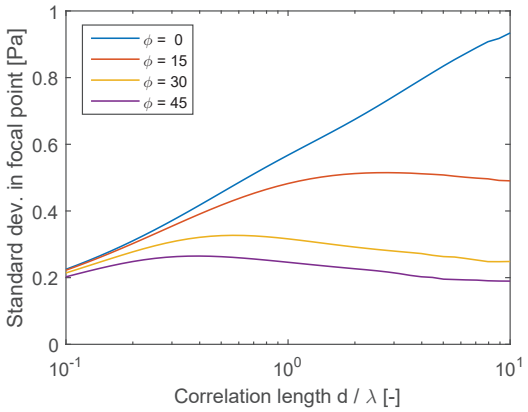

Figure 5: The standard deviation of the scattered field as the function of correlation length d for different angles

deviation of perturbations was selected as $\sigma = 1$ cm, and the correlation length was varied in the range $0.1 \leq d_{\text{corr}}/\lambda \leq 10$ logarithmically.

For each selected correlation lengths, 300 KL-modes were enough to represent the 95% of the standard deviation of the stochastic deformation. For one right hand side of the first order system, 50-90 iterations were needed for the GMRES algorithm to converge.

Figure 4 shows the magnitude of the scattered mean field, one realization of the perturbed field, and the standard deviation of the scattered field, assuming $\epsilon = 1$. The standard deviation is computed by the definition $\mathrm{D}_p(\mathbf{x}) = \sqrt{\mathrm{Cov}_p(\mathbf{x}, \mathbf{x})}$. The maximum of the standard deviation is at the focus point, its magnitude is 70% of the magnitude of the incident field. Figure 5 displays the standard deviation as a function of the correlation length d_{corr}. The blue curve ($\phi = 0$) corresponds to the focal point, the other curves display results measured at the focal distance, but with an inclination from the normal direction. In the normal case, the standard deviation increases with increasing correlation length. The explanation of this behavior is that the standard deviation of perturbations is kept constant.

Conclusions

We have demonstrated the application of the Fast Multipole Method for the solution of a stochastic scattering problem with uncertain geometry. It was shown that the FMM has twofold application in this field: (1) to solve the stochastic eigendecomposition problem with an iterative eigensolver, and (2) to solve consequent acoustic exterior problems with GMRES. The applied perturbation method has the advantage that the exterior problems are written for the same geometry, and the initialization of the FMM—which is the most time consuming part of the computation procedure—needs to be performed only once for one geometry and wave number. Furthermore, solution with right hand sides of decreasing significance can be optimized by relaxing the tolerance of the eigensolver, as well as reducing the accuracy of a single matrix-vector product in the FMM.

Acknowledgement

Emberi Erőforrások Minisztériuma

Supported by the ÚNKP-17-4-III New National Excellence Program of the Ministry of Human Capacities

References

[1] Raed Ghanem and Polhronis-Thomas Spanos. *Stochastic Finite Elements: A Spectral Approach*. Springer, New York, 01 2003.

[2] Ivo Babuška, Fabio Nobile, and Raúl Tempone. A stochastic collocation method for elliptic partial differential equations with random input data. *SIAM Journal of Numerical Analysis*, 45(3):1005–1034, 2007.

[3] H. Harbrecht and J. Li. First order second moment analysis for stochastic interface problems based on low-rank approximations. *ESAIM: Mathematical Modelling and Numerical Analysis*, 47:1533–1552, 2013.

[4] H. Harbrecht, R. Schneider, and Ch. Schwab. Sparse second moment analysis for elliptic problems in stochastic domains. *Numerische Mathematik*, 109:385–414, 2008.

[5] William Fong and Eric Darve. The black-box fast multipole method. *Journal of Computational Physics*, 228:8712–8725, 2009.

[6] W Crutchfield, Z Gimbutas, L Greengard, J Huang, V Rokhlin, N Yarvin, and J Zhao. Remarks on the implementation of the wideband FMM for the Helmholtz equation in two dimensions. *Contemporary Mathematics*, 408, 01 2006.

[7] P. Fiala and P. Rucz. NiHu: an open source C++ BEM library. *Advances in Engineering Software*, 75:101–112, 9 2014.